



# MICROMAGNETIC STUDY OF IRON NANOWIRE ARRAYS

CONSTANTIN DAVID<sup>1,2</sup>, WILHELM KAPPEL<sup>1</sup>, EROS-ALEXANDRU PĂTROI<sup>1</sup>, EUGEN MANTA<sup>1</sup>, VALENTIN MIDONI<sup>3</sup>

**Keywords:** Hysteresis curves, Micromagnetic model, Permanent magnet applications, Numerical simulations

Permanent magnets are essential components of various types of electric motors, generators, and other important technology. The strongest permanent magnets are made of rare earth metals. Examples of these rare earth magnets are the neodymium-iron-boron magnet (NdFeB) or the samarium-cobalt magnet (SmCo). However, permanent magnets rich in rare earth metals are expensive and thermally unstable. It would be extremely beneficial if permanent magnets could somehow be developed by using cheap and thermally stable transition metals. Cobalt nanowire arrays have been developed in the past by chemical methods and it has been found that this type of systems can exhibit large coercivities of up to almost 1 MA/m, which can become comparable with NdFeB/SmCo magnets at high temperatures. In this article micromagnetic simulations are used to study various iron nanowire arrays. Thus, it can be determined why these assemblies give rise to incredible magnetic properties. The advantage of micromagnetic simulations is the ability to analyze a broad range of geometries and materials and to get an insight into the physics behind the observed magnetic properties.

## 1. INTRODUCTION

The attention of the scientific community regarding electromagnetism has been directed in the last decades towards the study of ever smaller systems, such as micro- and nanoscopic ones [1]. In the light of this new trend, the implied physics changed to a combination between quantum physics and macroscopic physics, especially in what is known as micromagnetism [2]. Several studies show that using soft magnetic microscopic systems can lead to developing permanent magnets with little to no need for rare-earth components to be added [3,4]. Permanent magnets are key components of many types of applications such as actuators [5,6], motors, micro-motors [7], energy harvesters [8] and so on. Other studies focused on the design and simulation of large nanowire arrays, be they segmented or not, for they have promising applications in the realm of magnetic sensors, recording media, magnonic crystals [9,10], hard disk drives (HDD), magnetoresistive random access memories (MRAM) [1] and others such as a three-dimensional racetrack memory [11], spintronics [12] or micro-electro-mechanical systems (MEMS) [13]. Increased thermal stability makes nanowire arrays a perfect candidate for designing MEMS [14].

Multiple systems of different compositions (Fe, Co, Fe-Co, *etc.*) have been analyzed in previous research, such as spheroids, cylindrical nanowires – isolated or arrays, segmented (typically two parts with different magnetic properties and one non-magnetic part) or not, embedded in magnetic or non-magnetic matrices [3,14–18] and many others. The studies that focus on nanowire arrays can be categorized into three main classes – (i) the ones which focus on obtaining the nanowires, mainly through electrodeposition on nanoporous membranes such as anodic aluminum oxide (AAO) templates, and the characterization of their magnetic properties [19–24]; (ii) the ones which employ micromagnetic simulations to better understand magnetization reversal processes, nucleation, hysteresis loop formation [3,4,14,15,18,25,26]; (iii) the ones which deal with the interactions and reversal mechanisms in ferromagnetic nanowire arrays [27–33,17]. Most of the articles agree upon a few remarks, such as the fact that the coercive field

increases when the diameter gets smaller and smaller; the shape anisotropy of high aspect-ratio nanowires (length divided by diameter) makes the coercive field to stop from rising after a certain point ( $L/D \geq 10$  [34]), in which case the nanowires can be considered infinitely long; nucleation of cylindrical nanowires begins at the its ends through vortex states [3,14,26]. The interaction between interacting nanowires has been studied in several studies by using first-order reversal curve diagrams, FORC [28–33]. To obtain knowledge about the reversal mechanisms, the coercive field, and the rectangle degree (also known as squareness) of the hysteresis loops, defined as the remanent magnetization divided by the saturation magnetization ( $M_r/M_S$ ), have been studied [27]. More details about synthesis of nanowire arrays, magnetic properties and applications of cylindrical nanowires can be found in [27,35].

In this article we continue the studies on iron nanowire arrays with variable diameter, length, inter-wire distance and number – either finite or partially infinite – by numerically simulating their magnetization distribution, from which magnetic properties can be deduced. The purpose of this study is to further understand the magnetization reversal processes, hysteresis loop shapes and try, if possible, to extrapolate to what would happen at experimentally measurable systems.

## 2. NUMERICAL SIMULATION

In micromagnetism the main unknown is the magnetization distribution,  $\mathbf{M}$ . The goal of the micromagnetic model as far as statics is concerned is to discretize space and find  $\mathbf{M}$  at each discretization cell such that the total energy of the system, as given by various  $\mathbf{M}$  dependent factors, reaches a minimum [1,35]. The energy factors include cubic or uniaxial anisotropy

energy,  $E_{anic} = \int_{\Omega_m} K(m_1^2 m_2^2 + m_2^2 m_3^2 + m_1^2 m_3^2) dV$ , exchange

energy,  $E_{exchange} = \int_{\Omega_m} A(\nabla \mathbf{m})^2 dV$ , demagnetization energy,

$E_{demag} = -\frac{\mu_0}{2} \int_{\Omega_\infty} M_s \mathbf{m} \cdot \mathbf{H}_{dem} dV$ , the energy the systems has

<sup>1</sup> National Institute for R & D in Electrical Engineering ICPE-CA, 313 Splaiul Unirii, Bucharest, constantin.david@icpe-ca.ro

<sup>2</sup> Faculty of Electrical Engineering, Politehnica University of Bucharest 313 Splaiul Independenței, Bucharest

<sup>3</sup> SC MEDAPTEH PLUS CERT SRL, 27 Șelimbăr, Măgurele, Ilfov

when placed in an external magnetic field, known as the Zeeman energy term,  $E_{Zee} = -\mu_0 \int_{\Omega_m} M_s \mathbf{m} \cdot \mathbf{H}_{app} dV$  and other

terms [35]. Here,  $K$  is the cubic anisotropy constant,  $A$  is the exchange constant,  $M_s$  is the saturation magnetization,  $\mathbf{m}$  is the normalized magnetization,  $\mathbf{M}/M_s$ , and  $m_i = \mathbf{e}_i \cdot \mathbf{m}$ , with  $\mathbf{e}_i$  being one of the three anisotropy axis. To solve for  $\mathbf{m}$  one has to solve the following constraint optimization problem:  $\min(E_{tot}[\mathbf{m}])$  such that  $|\mathbf{m}(\mathbf{r})| = 1, \forall \mathbf{r} \in \Omega_m$ , where  $\Omega_m$  represents the domain of the magnetic material. One could also integrate in time the Landau-Lifshitz-Gilbert equation to obtain the relaxed state, but it is not efficient for computing hysteresis curves [36].

The equations of micromagnetism must be computed using numerical methods such as finite difference method (FDM), appropriate for rectangular geometries, or finite element method (FEM), appropriate for rounded geometries [36]. These methods are implemented in many available resources [2], but the one we have used in this paper is Ubermag [37,38], a Python interface for OOMMF [39], which uses FDM, a far less computationally intensive method than FEM. The ‘‘Ubermag’’ software is a collection of packages which allow for defining the problem to be solved in the Python ecosystem, while the actual calculations are done by the computational backend, which is OOMMF.

Iron parameters have been taken from reported values in various publications [1,26,34,40] as being  $M_s = 1.7 \cdot 10^6$  A/m,  $K = 0.48 \cdot 10^5$  J/m<sup>3</sup> and  $A = 21$  pJ/m. Discretization cells have been chosen such that the maximum length along a certain dimension is below

$$l_{ex} = \sqrt{\frac{2A}{\mu_0 M_s^2}} \cong 3.4 \text{ nm}, \text{ the exchange length [15] of iron.}$$

Other materials have been already studied in the past, out of which cobalt has shown interesting properties, such as high coercivity [41–43].

For every set of simulations, the discretization cells had the same dimensions, approximately 2 nm per dimension. The approximation of the curvature of the cylinders with cubic cells is a source of errors. To minimize errors, one must choose the diameter of the circular cross-section much larger than the dimensions of the discretization cell.

### 3. RESULTS AND INTERPRETATION

The first analyzed system consists of one  $L = 200$  nm long nanowire with its diameter  $D = 30$  nm placed in uniform magnetic field directed along the nanowire’s long axis. The hysteresis loop was constructed by sweeping the external magnetic field from a minimum value to a maximum value and back. To illustrate how shape anisotropy influences the magnetization distribution, we have also simulated the hysteresis curve for an applied field perpendicular to the easy axis of magnetization. The results of this simulation are shown in Fig. 1. From this figure it is deduced that when the applied field is along the easy axis, the magnetic moments are less likely to deviate from the parallel direction to minimize the total energy, but when the field switches sign and hits a critical point, all the magnetic dipoles turn at once, pointing again in the direction of the field. As opposed to this behavior, when the applied field is perpendicular to the easy axis, the squareness of

the loop is approximately zero. Both behaviors are due to the strong shape anisotropy of the high aspect-ratio nanowires.

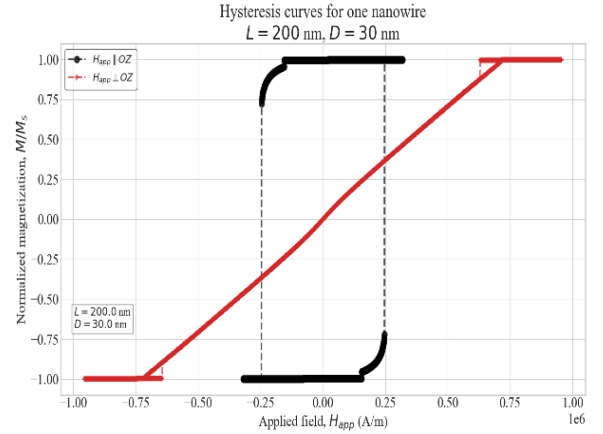


Fig. 1 – Hysteresis loops for one cylindrical nanowire; (black) – the applied field is parallel to the easy axis of magnetization; (red) – the applied field is perpendicular to the easy axis of magnetization.

Next, it has been investigated the behavior of the hysteresis curves of one nanowire with fixed diameter  $D = 30$  nm and variable length  $L$ . The hysteresis curves are plotted on the same graph in Fig. 2.

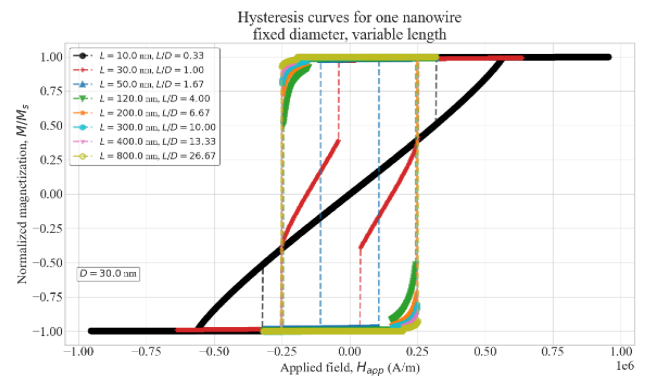


Fig. 2 – Hysteresis loops for one nanowire with fixed diameter  $D = 30$  nm and variable length; the applied field was taken along the length of the nanowire.

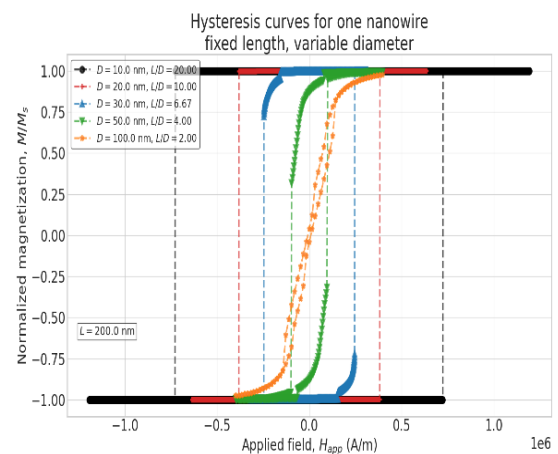


Fig. 3 – Hysteresis loops for one nanowire with fixed length  $L = 200$  nm and variable diameter; the external field was applied in the same direction as the length of the cylinder.

One thing that can be noticed is that, as reported in other studies, the coercive field remains constant as  $L/D$  grows above a certain threshold. The squareness of the loop goes closer to 1 as  $L/D$  grows above 13. Another thing is the

important role of the shape anisotropy energy – bigger aspect ratios lead to loops with higher squareness when applying the external field along the long axis.

The dependence of the coercive field on the diameter of the nanowire can be shown by plotting the hysteresis curves for cylinders with fixed length  $L = 200$  nm and variable diameter, as can be seen in Fig. 3. This figure proves that the coercive field decreases strongly with the increase of the diameter, behavior seen in other studies on multiple types of systems.

Finally for the one nanowire, Fig. 4 presents the magnetization distribution for an applied field value of  $-0.23$  MA/m. Here it can be seen that the magnetization reversal takes place by nucleation at the top and the bottom of the nanowire through vortex states.

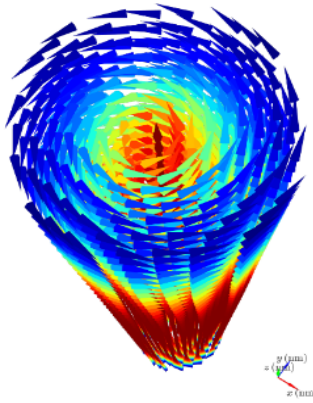


Fig. 4 – Magnetization distribution along one nanowire with  $L = 200$  nm,  $D = 30$  nm at an applied field value equal to  $-0.23$  MA/m; the color encodes the  $z$ -component of magnetization.

The second analyzed group of systems was the group of finite arrays of cylindrical nanowires. Here there are described results for  $n_x \times n_y$  arrays of nanowires with  $L = 250$  nm,  $D = 15$  nm and inter-wire spacing as measured from edge-to-edge  $\delta = 3$  nm. Here,  $n_x$  represents the number of nanowires along the  $x$ -axis and  $n_y$  stands for the number of nanowires along the  $y$ -axis.

The simulations were performed on  $1 \times 1$ ,  $2 \times 2$ ,  $3 \times 3$ ,  $4 \times 4$  and  $5 \times 5$  arrays of cylindrical iron nanowires. The hysteresis loops are shown in Fig. 5.

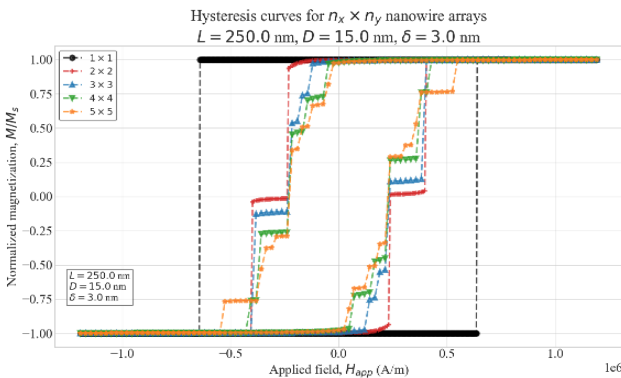


Fig. 5 – Hysteresis loops for finite nanowire arrays of  $1 \times 1$ ,  $2 \times 2$ ,  $3 \times 3$ ,  $4 \times 4$  and  $5 \times 5$  nanowires; they are arranged hexagonally and the inter-wire spacing was chosen to be 3 nm.

To get an idea of how the nanowires are arranged into the arrays, Fig. 5a shows the example of a  $3 \times 3$  array. The hysteresis loops are computed for the whole system of nanowires, as if they were enclosed in an air box. They

show that increasing the number of nanowires introduces some “steps” in the loops. Basically, at each step there is a certain number of nanowires that completely switch their magnetization from antiparallel to parallel with the applied field. Also, the hysteresis curves become more oblique-shaped as the number of nanowires grows, getting closer to how experimental data seen in other studies look like.

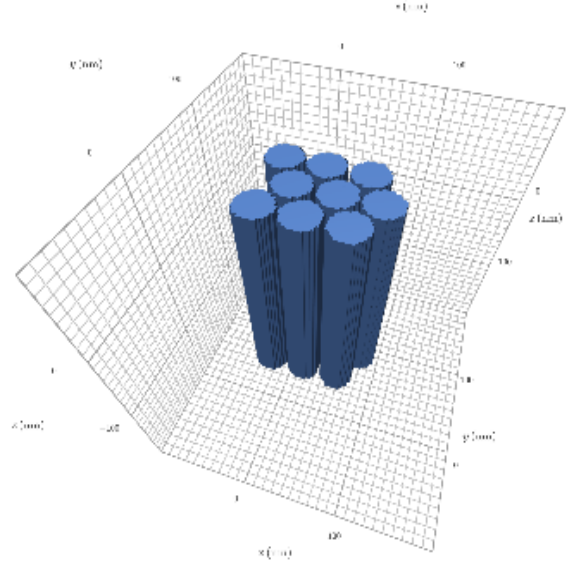


Fig. 5a – Geometry of a  $3 \times 3$  nanowire array.

The effect of demagnetization energy might be seen by varying the inter-wire distance. To that end, we have simulated  $2 \times 2$  arrays placed at various distances apart. The hysteresis curves can be seen in Fig. 6.

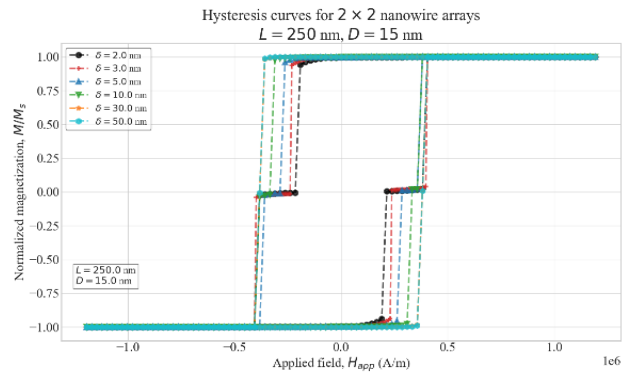


Fig. 6 – Hysteresis loops for a  $2 \times 2$  array of nanowires placed at various inter-wire distances,  $\delta$ , taken as the distance between the two closest edges of two neighboring nanowires.

A cross section through the top of the nanowires for the  $\delta = 3$  nm case at an applied field value where we see the intermediate state (magnetization is close to zero) is shown in Fig. 6a. This figure demonstrates that the intermediate state is characterized by two nanowires which have the magnetic moments pointing in the same direction as the applied field and two nanowires which have the magnetic moments pointing in the opposite direction. The blue ones will always be the first ones to switch in this configuration because the demagnetization field created by the neighboring nanowires will be higher on them than on the red ones and it will also be in the same direction as the applied field, which will result in a stronger effective field applied on the blue nanowires, so they switch faster. The

farther away the nanowires are placed from each other, the less the demagnetization field “helps” the applied field to switch the nanowires, so the switching field occurs at higher applied field values, as can be seen from Fig. 6.

The goal of this study was to simulate the behavior of infinite arrays of nanowires to be able to make implications about how experimental systems might behave. The infinite size along the  $y$ -axis was simulated by making use of Ubermag’s periodic boundary conditions, PBC.

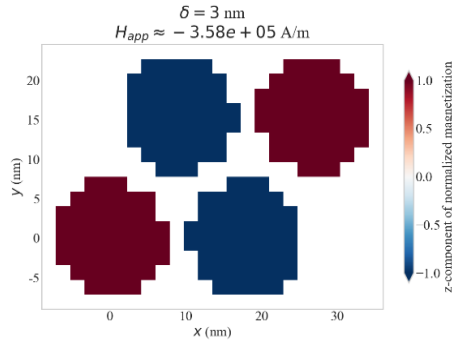


Fig. 6 – Hysteresis loops for a 2x2 array of nanowires placed at various inter-wire distances,  $\delta$ , taken as the distance between the two closest edges of two neighboring nanowires.

Figure 7 illustrates how PBCs are used. Firstly, the yellow shaded part is the original created system. The red circles represent the cross sections of the nanowires. This original system is then used to make identical copies along the  $y$ -axis, as are the gray shaded parts. This behavior simulates an infinite system along the  $y$ -axis. The image copies are placed such that the ensemble of original cell and image cells looks like how a real and very large system would be. The green hexagons are not part of the system, they were drawn to highlight the hexagonal geometry of the lattice. So far, PBCs along the  $x$ -axis cannot be applied because Ubermag does not support PBC along multiple dimensions coupled with using demagnetization energy. This feature might become available in the future, and we plan on using it to simulate a fully infinite system, as a single axis on which infinity cannot be achieved might not allow us to extrapolate to large arrays of nanowires due to edge effects.

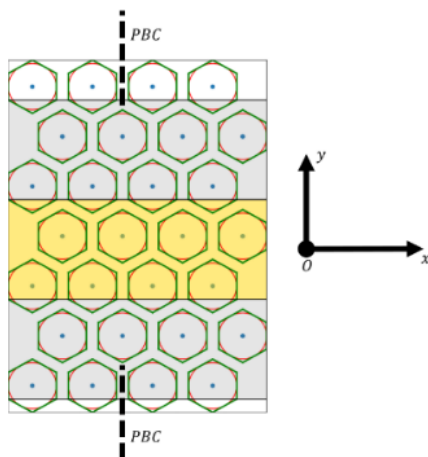


Fig. 7 – Image showing how nanowires are arranged to create infinite systems; yellow area shows original cell, gray areas show copies obtained with PBC.

To compensate for this fact, we have made multiple systems with increasing number of nanowires along the  $x$ -axis, trying to extrapolate to what would happen when this number goes to infinity, but it would be too

computationally intensive to add hundreds, or maybe thousands of nanowires along the  $x$ -axis, so the extrapolation might not be exact. The simulated hysteresis curves are shown in Fig. 8.

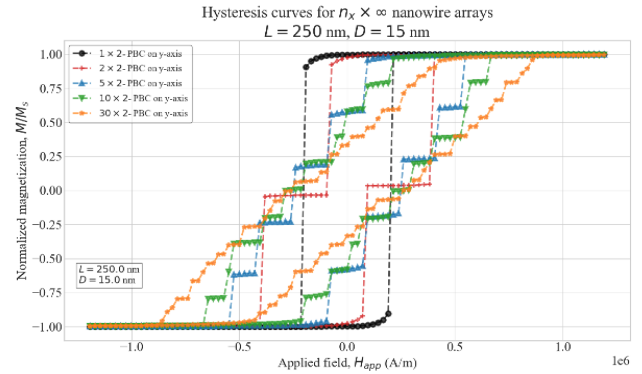


Fig. 8 – Hysteresis loops for partially infinite array of nanowires; infinity along the  $y$ -axis was obtained by means of PBC and along the  $z$ -axis was obtained by choosing an aspect-ratio bigger than 13. Along the  $x$ -axis we have simulated an increasing number of nanowires, up to 30.

The results show that the hysteresis curves become smoother and smoother as the number of nanowires along the  $x$ -axis increases. Also, analyzing the “30x2 – PBC on  $y$ -axis” case we can deduce the coercive field as being above 0.2 MA/m and the squareness well above 0.25, having a remanent polarization greater than 0.534 T. In experiments, cobalt nanowire arrays have been shown to be even better, the coercivities being somewhere between 0.5 MA/m to 1 MA/m [41–43], but more simulations need to be done to find geometries and material choices that are fitting the needs for permanent magnet applications.

#### 4. CONCLUSION

In conclusion, this study shows that structures with ferromagnetic nanowires could be designed such that they have suitable magnetic properties for developing permanent magnet-based applications. Simulations are important because they allow us to understand the underlying mechanisms behind hysteresis loops and associated magnetic properties, thus making possible designing systems with predictable properties. Here we found that high aspect-ratio interacting iron nanowires arranged in a hexagonal array could be a rare-earth free alternative for designing permanent magnets, but further investigations must be performed to have a clearer picture on what arrangement might prove to be the most efficient. Also, we plan on using a FEM approach to study cylindrical nanowires in the future, potentially applying PBC along all axes. Other plans include studying suitable materials for magnetic recording [44] and infinite arrays of  $\text{Fe}_3\text{O}_4$  nanoparticles as they have been shown to have important biomedical applications [45].

#### 5. ACKNOWLEDGEMENT

This study was possible by having the financial support from project PN no. 19310103 (5103)/2019, contract POC 133-D2/2018 and project no. 30 PFE/2018 between National R&D Institute for Electrical Engineering ICPE-CA and Romanian Ministry of Education and Research.

Received on November 11, 2021

## REFERENCES

1. R. Boardman, *Computer simulation studies of magnetic nanostructures*, 2005.
2. J. Leliaert, J. Mulkers, *Tomorrow's micromagnetic simulations*, J. of Applied Physics, **125**, pp. 180901, 2019.
3. S. Bance, J. Fischbacher, T. Schrefl, I. Zins, G. Rieger and C. Cassignol, *Micromagnetics of shape anisotropy based permanent magnets*, J. of Magnetism and Magnetic Materials, **363**, pp. 121-124, 2013.
4. S. Mahalingam, B. Manikandan and S. Arockiaraj, *Review – micromagnetic simulation using OOMMF and experimental investigations on nano composite magnets*, J. of Physics: Conference Series, **1172**, pp. 012070, 2019.
5. A. Radulian, M. Maricar, I. Nemoianu, R. Crețu, *New solution of linear dc actuator with additional permanent magnets: working principle, design and testing*, Revue Roumaine des Sciences Techniques - Serie Électrotechnique et Énergétique, **62**, 1, pp. 3-7, 2017.
6. R. Olaru, A. Arcire, C. Petrescu, *New linear actuator with ferrofluid and permanent magnets*, Revue Roumaine des Sciences Techniques – Serie Électrotechnique et Énergétique, **60**, 2, pp. 113-121, 2014.
7. M. Modreanu, M.-I. Andrei, M. Morega, T. Tiberiu, *Brushless dc micro-motor with surface mounted permanent magnets*, Revue Roumaine des Sciences Techniques – Serie Électrotechnique et Énergétique, **59**, 3, pp. 237-247, 2014.
8. R. Olaru, R. Gherca, C. Petrescu, *Analysis and design of a vibration energy harvester using permanent magnets*, Revue Roumaine des Sciences Techniques – Serie Électrotechnique et Énergétique, **59**, 2, pp. 131-140, 2014.
9. S. Agramunt-Puig, N. Del-Valle, E. Pellicer, J. Zhang, J. Nogue, C. Navau, A. Sanchez and J. Sort, *Modeling the collective magnetic behavior of highly packed arrays of multi-segmented nanowires*, New Journal of Physics, **18**, p. 013026, 2016.
10. M. Méndez, S. Gonzalez, V. Vega, J. Teixeira, B. Hernando, C. Luna, V. Prida, *Ni-Co alloy and multisegmented Ni/Co nanowire arrays modulated in composition: structural characterization and magnetic properties*, Crystals, **7**, p. 66, 2017.
11. J. Rial and M. Proenca, *A novel design of a 3D racetrack memory based on functional segments in cylindrical nanowire arrays*, Nanomaterials, **10**, pp. 2403, 2020.
12. E. Palmero, C. Bran, R. Real and M. Vázquez, *Synthesis and magnetism of modulated FeCo-based nanowires*, J. of Physics: Conference Series, **755**, pp. 012001, 2016.
13. A. C. Fischer, *Integration and fabrication techniques for 3D micro-and nanodevices*, 2012.
14. I. Dubitskiy, A. Almekaw, E. Iashina, S. Sotnichuk, K. Napolskii, D. Menzel, A. Mistonov, *Effect of interactions and non-uniform magnetic states on the magnetization reversal of iron nanowire arrays*, J. of Superconductivity and Novel Magnetism, **34**, pp. 539-549, 2020.
15. F. Zighem, T. Maurer, F. Ott, G. Chaboussant, *Dipolar interactions in arrays of ferromagnetic nanowires: a micromagnetic study*, J. of Applied Physics, **109**, 2010.
16. G. Nguyen Vien, S. Rioual, F. Gloaguen, B. Rouvellou, B. Lescop, *Study of the magnetization behavior of ferromagnetic nanowire array: Existence of growth defects revealed by micromagnetic simulations*, J. of Magnetism and Magnetic Materials, **401**, pp. 378-385, 2015.
17. D.-L. Sun, J.-H. Gao, X.-Q. Zhang, Q. Zhan, W. He, Y. Sun, Z.-H. Cheng, *Contribution of magnetostatic interaction to magnetization reversal of Fe 3Pt nanowires arrays: A micromagnetic simulation*, Journal of Magnetism and Magnetic, **321**, pp. 2737-2741, 2009.
18. W. Li, L. Zhao, Z. Liu, *Micromagnetic simulation on magnetic properties of Nd<sub>2</sub>Fe<sub>14</sub>B/a-Fe nanocomposites with Fe nanowires as the soft phase*, Frontiers of Materials Science, **12**, , pp. 348-353, 2018.
19. L. Zhang, Y. Zhang, *Fabrication, and magnetic properties of Fe<sub>3</sub>O<sub>4</sub> nanowire arrays in different diameters*, J. of Magnetism and Magnetic Materials, **321**, pp. L15-L20, 2009.
20. K. Nielsch, R. Hertel, R. Wehrspohn, J. Barthel, U. Gosele, S. Fischer, H. Kronmüller, *Switching behavior of single nanowires inside dense nickel nanowire arrays*, IEEE Transactions on Magnetics, **38**, pp. 2571-2573, 2002.
21. T. Sorop, C. Untiedt, F. Luis, L. J. Jongh, M. Kröll, M. Raşa, *Magnetization reversal of individual Fe nanowires in alumites studied by magnetic force microscopy*, J. of Applied Physics, **93**, pp. 7044-7046, 2003.
22. Q. Liu, J. Wang, Z. Yan, D. Xue, *The effect of diameter on micro-magnetic properties of Fe<sub>0.68</sub>Ni<sub>0.32</sub> nanowire arrays*, J. of Magnetism and Magnetic Materials, **278**, pp. 323-327, 2004.
23. C. Bran, Y. Ivanov, D. González Trabada, J. Tomkowicz, R. Real, O. Chubykalo-Fesenko, M. Vazquez, *Structural dependence of magnetic properties in Co-based nanowires: experiments and micromagnetic simulations*, IEEE Transactions on Magnetics, **49**, pp. 4491-4497, 2013.
24. Y. Ivanov, O. Chubykalo-Fesenko, *Micromagnetic simulations of cylindrical magnetic nanowires*, in Magnetic Nano- and Microwires: Design, Synthesis, Properties and Applications, pp. 423-448, 2015.
25. H. Li, M. Yue, Y. Peng, Y. Li, Q. Wu, W. Liu, D. Zhang, *Micromagnetic simulation of Co nanowires array*, in IEEE International Magnetics Conference (INTERMAG), pp. 1-1, 2017.
26. F. Ahmadi, M. Donahue, Y. Sozer, I. Tsukerman, *Micromagnetic study of soft magnetic nanowires*, AIP Advances, **9**, p. 125047, 2019.
27. M. Vazquez, *Magnetic Nano- and Microwires*, Woodhead Publishing Series in Electronic and Optical Materials, 2020.
28. L. Spinu, A. Stancu, C. Radu, F. Li, J. Wiley, *Method for magnetic characterization of nanowire structures*, IEEE Transactions on Magnetics, vol. 40, pp. 2116 - 2118, 2004.
29. C.-I. Dobrotă, A. Stancu, *What does a first-order reversal curve diagram really mean? A study case: array of ferromagnetic nanowires*, J. of Applied Physics, **113**, p. 043928, 2013.
30. F. Béron, D. Menard, A. Yelon, *First-order reversal curve diagrams of magnetic entities with mean interaction field: A physical analysis perspective*, J. of Applied Physics, **103**, pp. 07D908-07D908, 2008.
31. A. Rotaru, J.-H. Lim, D. Lenormand, A. Diaconu, J. Wiley, P. Postolache, A. Stancu, L. Spinu, *Interactions and reversal-field memory in complex magnetic nanowire arrays*, Phys. Rev. B, **84**, 13, pp. 134431, 2011.
32. L. Vivas, M. Vazquez, J. Escrig, S. Allende, D. Altbir, D. Leita, J. Araujo, *Magnetic anisotropy in CoNi nanowire arrays: analytical calculations and experiments*, Physical Review B, **85**, p. 035439, 2012.
33. M. Salem, P. Sergelius, R. Corona, J. Escrig, D. Görlitz, K. Nielsch, *Magnetic properties of cylindrical diameter modulated Ni 80Fe<sub>20</sub> nanowires: interaction and coercive fields*, Nanoscale, **5**, pp. 3941-3947, 2013.
34. H. Xiang, D. M. Jiang, J. C. Yao, Y. P. Zheng, W. Lu, G. Q. Li, H. Saito, S. Ishio, X. W. Tan, Y. Q. Lin, *Micromagnetic simulations of magnetization reversal of iron nanowire*, J. of Physics: Conference Series, **266**, p. 012022, 2011.
35. M. Stano, O. Fruchart, *Magnetic nanowires and nanotubes*, Handbook of Magnetic Materials, **27**, pp. 155-267, 2018.
36. C. Abert, *Micromagnetics and spintronics: models and numerical methods*, The European Physical Journal, **B**, **92**, p. 120, 2019.
37. M. Beg, R. Pepper, H. Fangohr, *User interfaces for computational science: a domain specific language for OOMMF embedded in Python*, AIP Advances, **7**, 2016.
38. M. Beg, R. A. Pepper, T. Kluyver, J. Mulkers, J. Leliaert, H. Fangohr, *Ubermag/Ubermag: meta package for Ubermag project*, Zenodo, <https://doi.org/10.5281/ZENODO.3539496>, 2019.
39. H. Kim, C.-Y. You, *Embedded object-oriented micromagnetic frame (OOMMF) for more flexible micromagnetic simulations*, J. of Magnetics, **21**, pp. 491-495, 2016.
40. Y. Ivanov, M. Vázquez, O. Chubykalo-Fesenko, *Magnetic reversal modes in cylindrical nanowires*, J. of Physics D, Applied Physics, **46**, 48, paper 48500, 2013.
41. K. Gandha, K. Elkins, N. Poudyal, X. Liu, J. P. Liu, *high energy product developed from cobalt nanowires*, Scientific reports, **4**, pp. 5345, 2014.
42. T. Maurer, F. Ott, G. Chaboussant, Y. Soumare, J.-Y. Piquemal, G. Viau, *Magnetic nanowires as permanent magnet materials*, Applied Physics Letters Volume, **91**, 17, pp. 172501, 2007.
43. K. Gandha, J. Mohapatra, J. P. Liu, *Coherent magnetization reversal and high magnetic coercivity in Co nanowire assemblies*, J. of Magnetism and Magnetic Materials, **438**, 2 pp. 41-45, 017.
44. A. Bordianu, V. Ioniță, L. Petrescu, *Micro-scale numerical simulation of the magnetic recording*, Revue Roumaine des Sciences Techniques – Serie Électrotechnique et Énergétique, **57**, 1, pp. 3-9, 2012.
45. V. Ioniță, I. Covaliu, L. Petrescu, A. Bordianu, O. Tabără, *Magnetic characterization of Fe<sub>3</sub>O<sub>4</sub> nanoparticles used in biomaterials*, Revue Roumaine des Sciences Techniques – Serie Électrotechnique et Énergétique, **57**, 2, pp. 154-161, 2012.